

Plasma Perturbations in High-Speed Probing of Hall Thruster Discharge Chambers: Quantification and Mitigation

Benjamin A. Jorns* Dan M. Goebel[†] and Richard R. Hofer[‡]

Jet Propulsion Laboratory, California Institute of Technology, Pasadena, CA 91109

An experimental investigation is presented to quantify the effect of high-speed probing on the plasma parameters inside the discharge chamber of a 6-kW Hall thruster. Understanding the nature of these perturbations is of significant interest given the importance of accurate plasma measurements for characterizing thruster operation. An array of diagnostics including a high-speed camera and embedded wall probes is employed to examine in real time the changes in electron temperature and plasma potential induced by inserting a high-speed reciprocating Langmuir probe into the discharge chamber. It is found that the perturbations onset when the scanning probe is downstream of the electron temperature peak, and that along channel centerline, the perturbations are best characterized as a downstream shift of plasma parameters by 15-20% the length of the discharge chamber. A parametric study is performed to investigate techniques to mitigate the observed probe perturbations including varying probe speed, probe location, and operating conditions. It is found that the perturbations largely disappear when the thruster is operated at low power and low discharge voltage. The results of this mitigation study are discussed in the context of recommended methods for generating unperturbed measurements of the discharge chamber plasma.

I. Introduction

The ability to qualify Hall effect thrusters for deep space applications strongly depends on the accuracy of the plasma properties in these devices. This is because the required thruster lifetime for many proposed missions¹⁻³—50,000 hrs in some cases—can only be validated in a cost-effective way through modeling. Hall thruster models in turn must be informed and validated by empirical measurements of thruster plasma properties. An adverse consequence for this dependence on plasma measurements most recently came to light during a demonstration of magnetic shielding technology on a 6 kW Hall thruster.⁴⁻⁶ Two different techniques for measuring the electron temperature along the channel centerlines of this thruster—embedded wall probes and a high-speed reciprocating probe—yielded two electron temperature profiles, each displaced from one another by 10-15% the length of the discharge chamber. This posed a significant problem: which measurement, if either, should be used to benchmark the thruster model? Normally, a 10% uncertainty may not be a concern for modeling a standard configuration Hall thruster; however, since magnetic shielding relies on exercising a high degree of control on the location of the plasma, this uncertainty represented a potential concern. Indeed, it was found that without trying to correct for this shift, it was not possible to capture simultaneously the experimentally measured spatial dependence of both plasma potential and electron temperature in the shielded configuration.

Probe-induced perturbations in the local plasma parameters may be to blame for the discrepancy between measurements noted in Refs. 4-6. Previous experimental studies on other Hall thrusters have showed that injecting probes into the discharge chamber can result in significant changes in the global operating parameters—most notably discharge current and cathode to ground potential.⁷⁻⁹ Even when these probes

*Engineer, Electric Propulsion Group, AIAA Member, benjamin.a.jorns@jpl.nasa.gov

[†]Senior Research Scientist, Thermal and Propulsion Engineering Section, AIAA Fellow

[‡]Senior Engineer, Electric Propulsion Group, AIAA Associate Fellow

are inserted at high-speed so as to minimize the ablation that can result from prolonged exposure to the plasma, other effects such as secondary electron emission from the probe body have been shown to impact the global operating parameters.¹⁰ The observation that probing can shift global operating parameters suggests that the local plasma properties—electron temperature and plasma potential—also may change. There is an open question, however, as to the nature and extent of these perturbations. This is a particularly important concern for the shielded 6-kW class thruster due to the reasons outlined above.

The purpose of this investigation is to provide a quantifiable measure of these perturbations by examining in real time the changes in the plasma parameters that are induced by high-speed probing of a 6 kW Hall thruster. In the first section, we outline the experimental setup and diagnostics we employed to quantify changes in the thruster plasma. In the second section, we present results that illustrate how probe insertion can alter both global thruster operating conditions and local measurements of electron temperature and plasma potential in the thruster channel. We follow this with a parametric investigation to determine what parameters—including probe speed, location, and thruster operating conditions—can impact the degree of the perturbations. In the third section, we discuss our results in the context of identifying what mechanism drives the probe-induced changes in the plasma. We then outline potential mitigation techniques that may be employed to generate accurate internal plasma measurements.

II. Experimental Setup

The goal of this experimental investigation was to quantify the effect that a scanning probe has on local plasma parameters as it translates axially into the discharge chamber. To this end, we employed a high-speed translating probe and an array of other diagnostics to monitor in real time the operating parameters and local plasma parameters. We describe these diagnostics in the following section as well as the thruster we investigated and the facility where the trials were performed.

A. Facility

We performed all of the experimental trials in the Owens Chamber located at the Jet Propulsion Laboratory (JPL). This facility is a 3 m × 10 m cylindrical vacuum chamber cryogenically-pumped to a base pressure of 5×10^{-7} torr. At the maximum ~ 19.5 mg/s flow rate of xenon employed in this set of trials, we measured the background pressure at $P_B = 1.5 \times 10^{-5}$ torr, which indicated a total pumping speed of approximately 170 kl/s at a standard temperature of 0° C .

B. Thruster

For this study, we investigated the H6US,^{5,6} a 6-kW Hall thruster (Fig. 1) jointly developed by the Air Force Research Laboratory, JPL, and the University of Michigan. The H6US has been thoroughly investigated experimentally and noted for its high performance and reliability.^{11–16} It employs boron nitride rings and a lanthanum hexaboride, center-line mounted cathode,¹⁷ operated at 7% anode flow. We chose to perform the campaign on this thruster as opposed to the H6MS, the magnetically shielded version of this thruster discussed in Refs. 5, 6, 18 and alluded to in Sec. I, since the acceleration zone in this device is sufficiently close to the exit plane that wall probes can resolve the location of the electron temperature maximum in the channel. In the magnetically shielded version, the plasma is displaced downstream such that wall probes do not yield significant information on the spatial dependence of the electron temperature. Since the discrepancy between measurement techniques outlined in Refs. 5 and 6 persisted for both variations of the thruster (H6US and H6MS), we opted for the unshielded configuration for this study.

C. High-speed translating probe

We employed a translating single Langmuir probe for our internal measurements of the H6US. This configuration previously was implemented at JPL to obtain electron temperature profiles for a number of different Hall thrusters including the H6US, and it was measurements from this setup that gave rise to the difficulties mentioned in the introduction in trying to match data to simulation results for the H6MS,^{5,6} a magnetically-shielded version of the H6US. It is because of this heritage and our interest in determining the impact of this probing technique on the H6US that we continued to adopt this configuration. In this setup, a Langmuir probe is mounted on a two-axis translation system (Fig. 2(a)) with belt-driven stages capable of moving

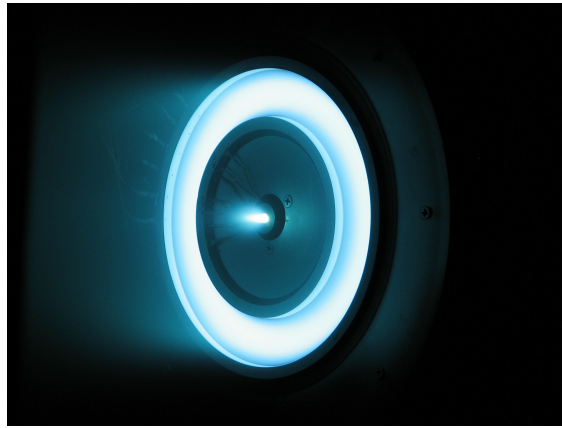


Figure 1: H6US installed at Owens chamber and operating at 300 V and 6 kW. Wall probes are located between the 9:00 and 12:00 positions.

at high speed (~ 1 m/s) in the axial direction. The exposed tip of the Langmuir probe is tungsten with a 0.25 mm diameter and 1.5 mm in length. The probe body is alumina, but we enclosed the 2.5 cm length of the body closest to the tungsten tip in a boron nitride (BN) sheath. This was done to minimize probe perturbation effects due to secondary electron emission and resulted in a probe width equal to $\sim 7\%$ of the channel width.

When collecting data with the translating system, the probe was first moved to a fixed radial position downstream of the thruster. It was then shot into the channel and quickly retracted. The typical shot length was approximately 100 ms with a residence time in the thruster channel of ~ 20 ms. In order to generate the characteristic Langmuir I-V trace, we first allowed the probe to float and recorded the potential as it shot into the thruster channel. We then employed for subsequent shots an arbitrary waveform generator in conjunction with a bi-operational amplifier to impose voltage sweeps on the floating potential profile. This technique permitted us to sweep through the ion saturation and plasma potential locally without driving the probe too far into electron saturation.



(a)



(b)

Figure 2: (a) High-speed translation stage installed in Owens chamber with mounted Langmuir probe. (b) Single Langmuir probe with boron nitride sheath.

The potential that we superimposed on the floating potential was a single-sided ramp with a frequency of 300 Hz and a 75% duty cycle. We chose this relatively low sweep rate and shape in order to minimize capacitive effects that we found would occur when applying a continuous, high frequency sinusoid. In order

to extract electron temperature from the I-V traces, we applied the semi-log plot technique (c.f. Ref 19) to the measured probe current in the vicinity of each trace’s floating potential. We also used the knee method to estimate the plasma potential. Since the probe was translating during the probe sweeps, each measurement had an inherent spatial uncertainty given by the distance the probe traveled when taking the sweep. On average, this positional error was ~ 1 mm, though the resolution of the individual data points was lower than this—the 300 Hz sweep rate only yielded 32 I-V traces per probe injection. We triggered the data acquisition system off position so that we could take the same I-V traces at the same spatial locations over multiple shots. As a consequence, we were able to average over multiple I-V traces to reduce noise. The electron temperatures reported in this work each represent the average of five axial injections.

D. Wall probes

We employed ten, single Langmuir probes embedded in the thruster boron nitride rings as a non-invasive diagnostic for electron temperature and plasma potential in the H6US. We show these probes in Fig. 3 arranged in the same configuration as outlined in Refs. 6 and 20 . The left side of this figure also depicts the magnetic field lines that intersect each wall probe. As we will discuss in Sec. III.B, we took advantage of the isothermality of field lines in the thruster channel to use these intersecting lines to map the electron temperature measured at the wall probes to different spatial locations in the plasma.

The exposed elements of the probes were tungsten, 0.5 mm in diameter, and installed flush with the boron nitride ring surface. They were clocked azimuthally from 9:00 to 12:00 and located from 0.85 L to 0.97 L downstream from the anode, where L denotes the length of the discharge chamber. This azimuthal clocking was implemented in order to minimize interference between the probe tips. During high-speed shots, the translating probe entered the plane at the 9:00 position, but it is assumed that any perturbations it induced at this azimuth were quickly communicated throughout the discharge chamber. This is a justified assumption given that $\tau_{E \times B} / \tau_p \ll 1$, where $\tau_{E \times B}$ is the time an electron driven by $E \times B$ drift requires to transit the channel azimuthally and τ_p is the translation time of the probe.

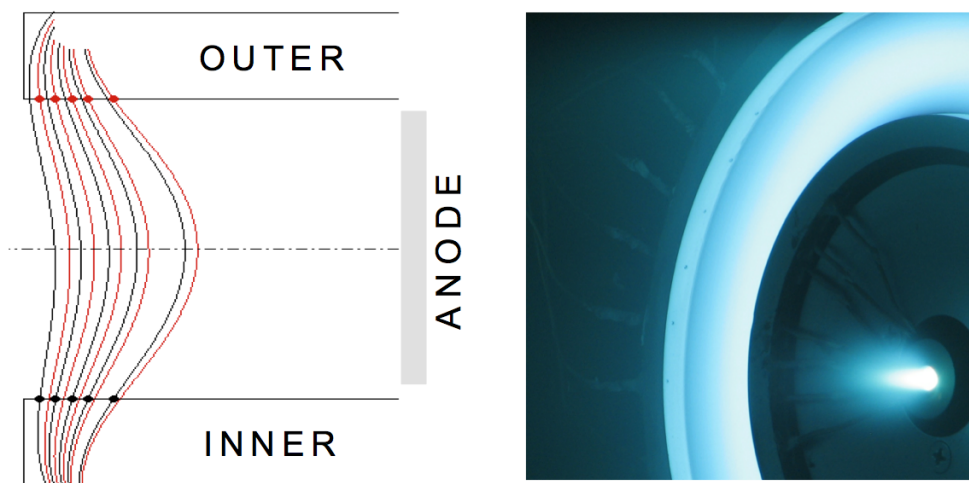


Figure 3: Left: Schematic for wall probes installed in the H6US with imposed magnetic field lines. Right: Zoomed in image of the mounted wall probes on the H6US during operation.

The presence of the wall probes is non-perturbative when compared to the effect of the translating probe entering the discharge chamber. This is because the insulator for these probes is the pre-existing boron nitride ring. No new elements are introduced to the thruster environment that would provide additional secondary electron effects or that could interrupt the electron current. There is of course the possibility that the act of sweeping the voltage to generate I-V traces could perturb the plasma—particularly by drawing large electron current—and so to mitigate this effect, we limited the maximum voltage on these probes to not exceed significantly the plasma potential.

The wall probes were employed to measure the impact of inserting the translating probe into the plasma. To this end, as the translating probe shot toward the anode, we took I-V traces on one of the 10 wall probes at 50 Hz, a slower sweep rate than we employed with the injected probe. This was necessary since parasitic capacitance for these wall probes was significantly higher than the translating probe (due in large part to their proximity to the grounded thruster body). At this lower, 50 Hz sweep rate, we were able to take ~ 6 I-V traces as the injected probe entered the thruster body. The sweeping on these probes was triggered by the position of the translation probe and was highly repeatable. This repeatability permitted us to measure the electron temperature on one probe at a time and still reconstruct the spatial distribution of electron temperature along the inner and outer rings as a function of translating probe position. We averaged over five shots with the translating probe for each wall probe measurement. This translated to a total of 25 required shots into the chamber in order to reconstruct the evolving spatial distribution of electron temperature along a given wall.

E. High speed camera

We employed a Photron FASTCAM SA1 high-speed camera to image the trajectory of the translating probe as it entered the H6US discharge chamber. It was installed with a view across the thruster face, and it operated at a frame rate of 12 kHz. The FASTCAM was triggered by the same probe position as the scanning Langmuir probe data acquisition system.

F. Operating condition diagnostics

We monitored two global thruster operating parameters during this investigation—the cathode to ground potential and discharge current oscillations. We measured the latter with a Pearson coil. Both of these parameters changed during probe injection, which provided further quantitative evidence of the nature of the probe-induced perturbations.

III. Results

In the following section, we describe the experimental results of our investigation into the perturbative effects of probing the discharge chamber. We present data demonstrating how both the global parameters and local plasma parameters were impacted by the probe shots.

A. Perturbations in global parameters

We show in Fig. 4 two FASTCAM video frames that were taken when the H6US operated at 300 V and 6 kW and the translating probe was injected into the channel on the side of the thruster opposite the camera. These stills serve to illustrate visually that not only does probe insertion perturb the plasma but that it appears to do so by shifting the plume from a collimated mode toward a configuration directed toward the centerline. Given the starkness of this visual transition, we would expect that the perturbation also should be indicated by other global thruster parameters. To examine this possibility, we reduced the information in the high speed images to a single parameter—the total pixel intensity from each frame—and plotted it as a function of translating probe position. At the same time, we plotted the cathode to ground potential and the RMS of the discharge current oscillations. The result is shown in Fig. 5 where the distances have been normalized by the length of the thruster channel and for reference we have indicated the location of the peak magnetic field as a dashed line.

Significantly, the global operating parameters—light intensity, cathode to ground potential, and the discharge oscillations—all exhibit a nearly binary transition. As the translating probe on centerline passes a threshold point at $Z \approx 0.8 L$ where Z is the distance from anode, these background parameters exhibit an immediate shift from one steady-state operating point to another. The cathode to ground potential increases, the light intensity decreases, and the discharge current oscillation amplitude decreases. The form and type of these transitions are consistent with the observations reported in the probe studies done in Refs. 8 and 10 for lower power thrusters, and taken together, they serve to show that probe insertion undoubtedly impacts global parameters of thruster operation in the H6US. It is reasonable to conclude then that if these parameters are changed, the local plasma parameters may also be impacted. We investigate this possibility in the next section.

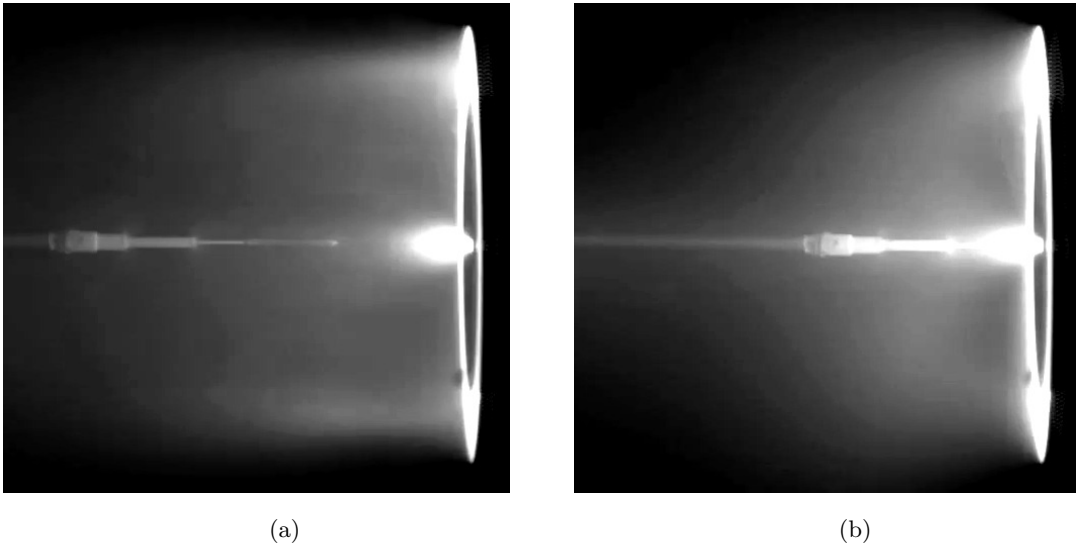


Figure 4: Stills sampled from the FASTCAM as the translating Langmuir probe enters the discharge chamber. (a) The probe is upstream and not perturbing the plasma. (b) The probe has entered the plasma and the light intensity profile correspondingly has shifted.

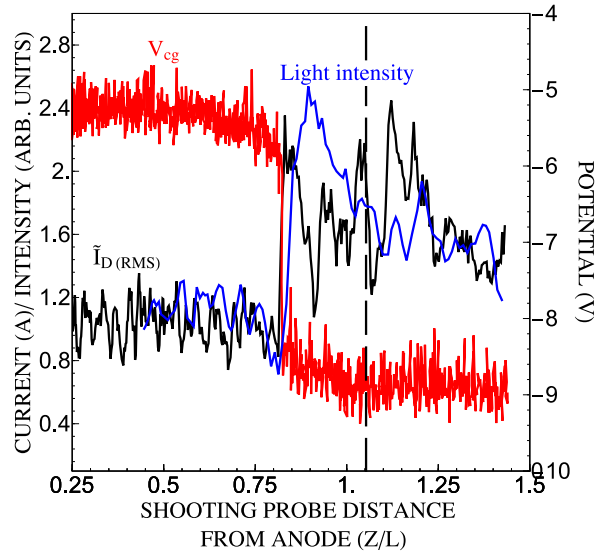


Figure 5: Global operating conditions including the total light intensity observed by the FASTCAM, the cathode to ground potential, V_{cg} , and the RMS of the discharge current, $\bar{I}_{D(RMS)}$, as a function of the translating probe's distance from anode. The thruster operating condition was 300 V at 6 kW, and the probe was injected on channel centerline. The dashed line denotes the location of peak radial magnetic field on centerline.

B. Perturbations in plasma parameters

As we outlined in Sec. II.D, we used wall probes to examine how the electron temperature and plasma potential at the inner and outer rings changed as the scanning probe entered the discharge chamber. We show the results of this study in Fig. 6 where we plot for the nominal case of 300 V and 20 A the electron temperature (a and b) and plasma potential (c and d) along both walls as a function of the scanning probe

distance for anode. Here the horizontal axis corresponds to the position of the translating probe with respect to the anode, and the vertical axis is the distance of the wall probe from the anode. A vertical line drawn through this plot represents the spatial distribution along the wall of the indicated plasma parameter when the injected probe was located at the point given by the intersection of the vertical line and the horizontal axis.

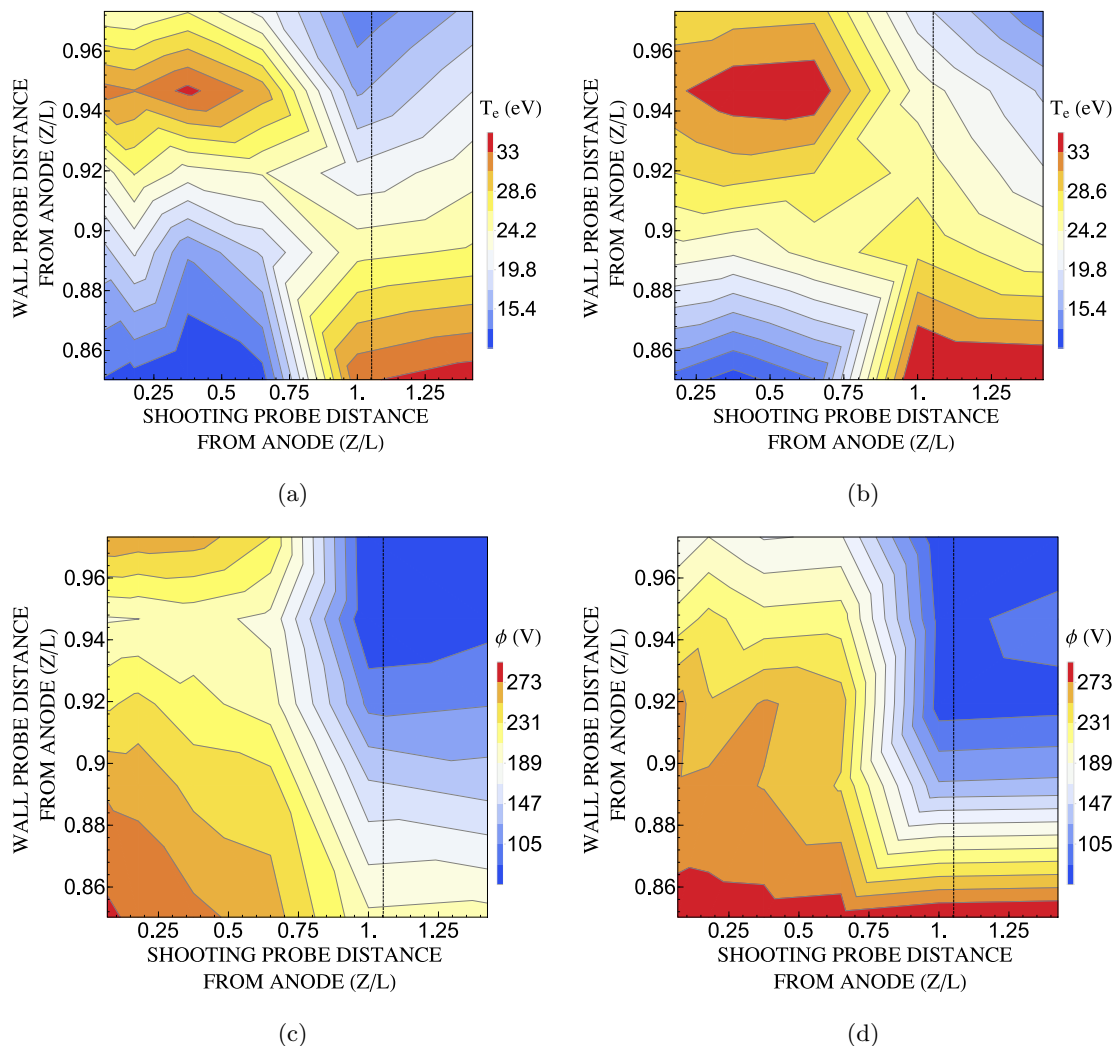


Figure 6: Plasma parameter profiles along the inner and outer rings as a function of the injected probe distance from the anode: (a) Electron temperature at the outer wall; (b) electron temperature at the inner wall; (c) plasma potential at the outer wall (d) plasma potential at the inner wall. The injected probe was along centerline for all the cases shown, and the dotted line in each figure denotes the location of peak radial magnetic field.

It is immediately evident from these results that the probe insertion induces a shift in the spatial dependence of the plasma parameters along the inner and outer walls. This transition occurs at the same location noted in Fig. 5 and exhibits the same binary character whereby the introduction of the probe moves the plasma to a new state. We can take advantage of this apparent shift between two steady-states to show in a simplified form the effect of introducing the probe to the discharge chamber. To this end, we average the electron temperature measurements over the points where the probe was downstream of the transition (the unperturbed points for $Z > 1$ L) and where the probe was upstream of the transition (the perturbed state from $Z = 0 - 0.8$ L). By plotting these averaged profiles in Fig. 7, we can see that in most cases the electron and plasma profiles contort in a way best described as a 10% L downstream shift. There is one exception to this characterization, which is the downstream uptick in plasma potential exhibited in the perturbed state

shown in Fig. 7(d). While we are confident that this is a valid data point, it is not consistent with how a simple downstream shift in potential would appear (c.f. Fig. 7(c)). Thus, even though the description of the perturbation as a downstream shift appears to be apt, we keep in mind that the magnitude and gradients in the plasma parameters also may be changing.

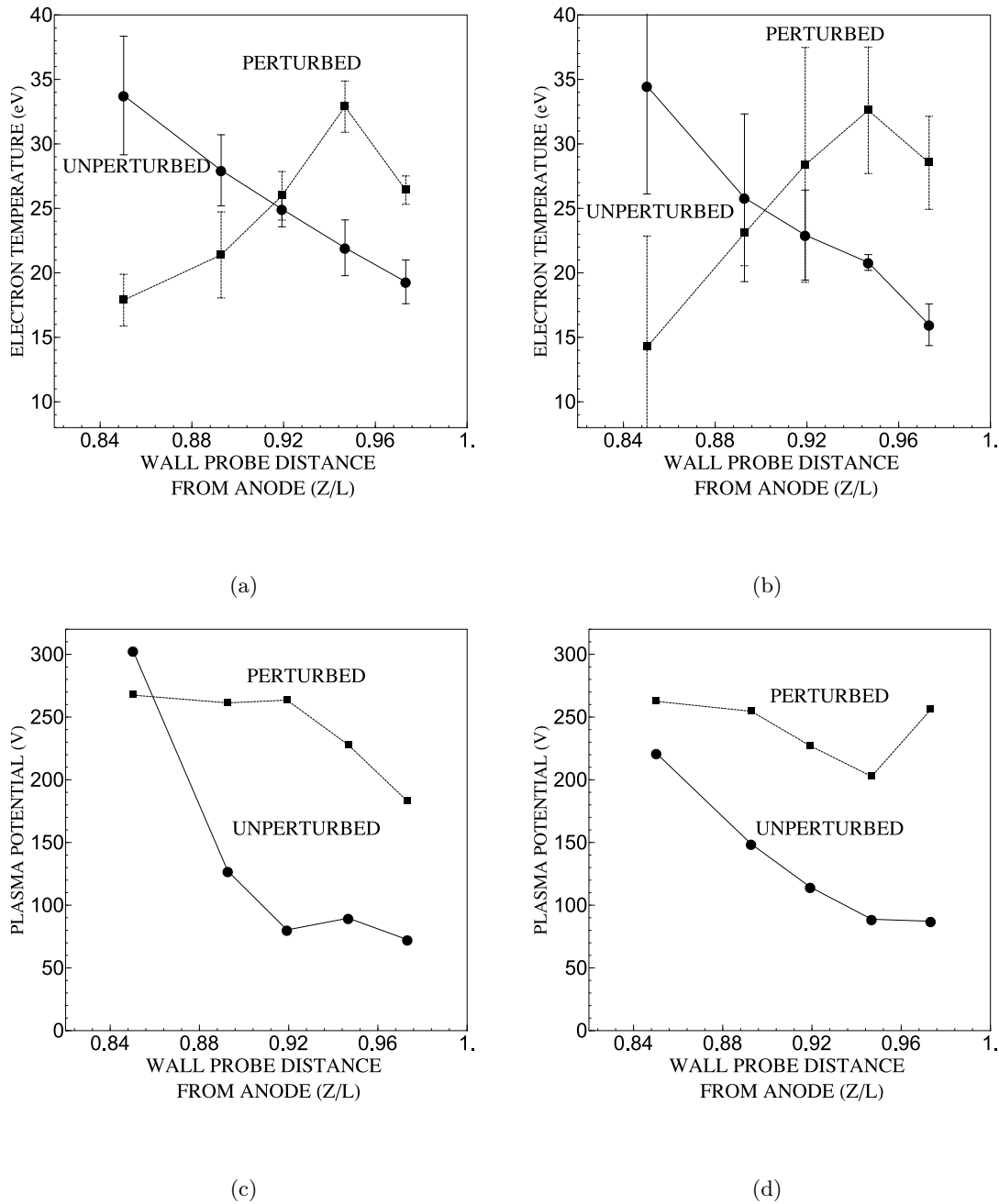


Figure 7: The average spatial dependence of the plasma parameters at the rings before and after the probe-induced transitions: (a) Electron temperature at the outer wall; (b) electron temperature at the inner wall; (c) plasma potential at the outer wall (d) plasma potential at the inner wall.

While the wall probe measurements serve as proof of the perturbative effect of the injected probe, our study is driven by an interest in how the plasma changes where the scanning probe actually takes data, the centerline. To examine this effect, we invoke the isothermality of magnetic field lines to map the electron temperature at the walls to the channel centerline. This is accomplished following the technique of Ref. 5 in

which we identify the magnetic field lines that intersect each probe (Fig. 3.) and map the temperature along these lines into the discharge chamber. The result of applying this method is shown in Fig. 8 along with electron temperature values at centerline inferred from the translating probe. In this plot, we have grouped the scanning probe measurements taken downstream of the transition point ($Z > 1$ L) with the unperturbed wall data and the data upstream of this point ($Z < 0.8$ L) with the perturbed wall probe data. In so doing, we immediately can see that the electron temperature profile is shifted by approximately 20% the length of the discharge chamber between the perturbed and unperturbed states. This displacement is larger than what we observed at the walls, though such an increase is not unexpected given how the intersecting magnetic field lines bow into the channel (Fig. 3). This observed 20% shift resolves the previously unexplained discrepancy between wall and scanning probe data previously cited in Refs. 4–6. It similarly eliminates any ambiguity in choosing the correct temperature profile to benchmark simulations of the thrusters. Indeed, this result would suggest that wall probe data complimented by unperturbed centerline probe data is the most accurate metric.

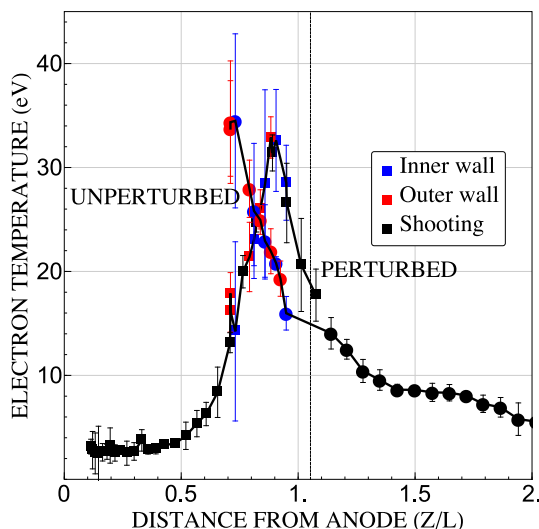


Figure 8: Wall probe electron temperatures mapped to the channel centerline overlaid with measurements performed with the scanning probe. The perturbed and unperturbed profiles are shown. The dashed line denotes the location of peak magnetic field.

C. Mitigation study

The results of the previous section have served to establish that the very act of probing the plasma can perturb it. And while we have identified a promising technique for capturing at least part of the unperturbed temperature profile—employing a combination of wall probes and injected probes—this technique has its own limitations. As can be seen from Fig. 8, the unperturbed profile does not actually indicate where the peak in electron temperature should be—the inflection never changes. This is because the wall probes did not extend sufficiently far upstream to capture the maximum. Additionally, while the isothermality of field lines allowed us to combine in an effective way the wall and injected probe data, this same technique is not applicable for plasma potential measurements. Since the field lines are not necessarily at equipotential, we are not able to use wall probes to infer the plasma potential profile upstream of the transition point. Ultimately, we would like unperturbed profiles of both plasma parameters along the entire length of the discharge chamber, but this begs the question: is there a way we can achieve this measurement? We identify three methods in this section that could facilitate this end: performing measurements off centerline, changing the probe speed, and varying operating conditions. We justify these techniques in the following and present the results from a parametric study of each.

1. Effect of probe radial location

The results of the Sec. III.B showed that the insertion of the translating Langmuir probe along the centerline shifted the plasma, but it possible that shots along other radial locations may be less perturbative. This is because the plasma is less dense near the walls, and if the plasma parameter shifts are in part driven by particle flux to the probe, injecting the probe axially at a radial location may reduce the perturbative effect. If this proves to be the case, then we could exploit the isothermality of lines to map the off-center shots to the centerline and in this way provide the measurements necessary to benchmark the code.

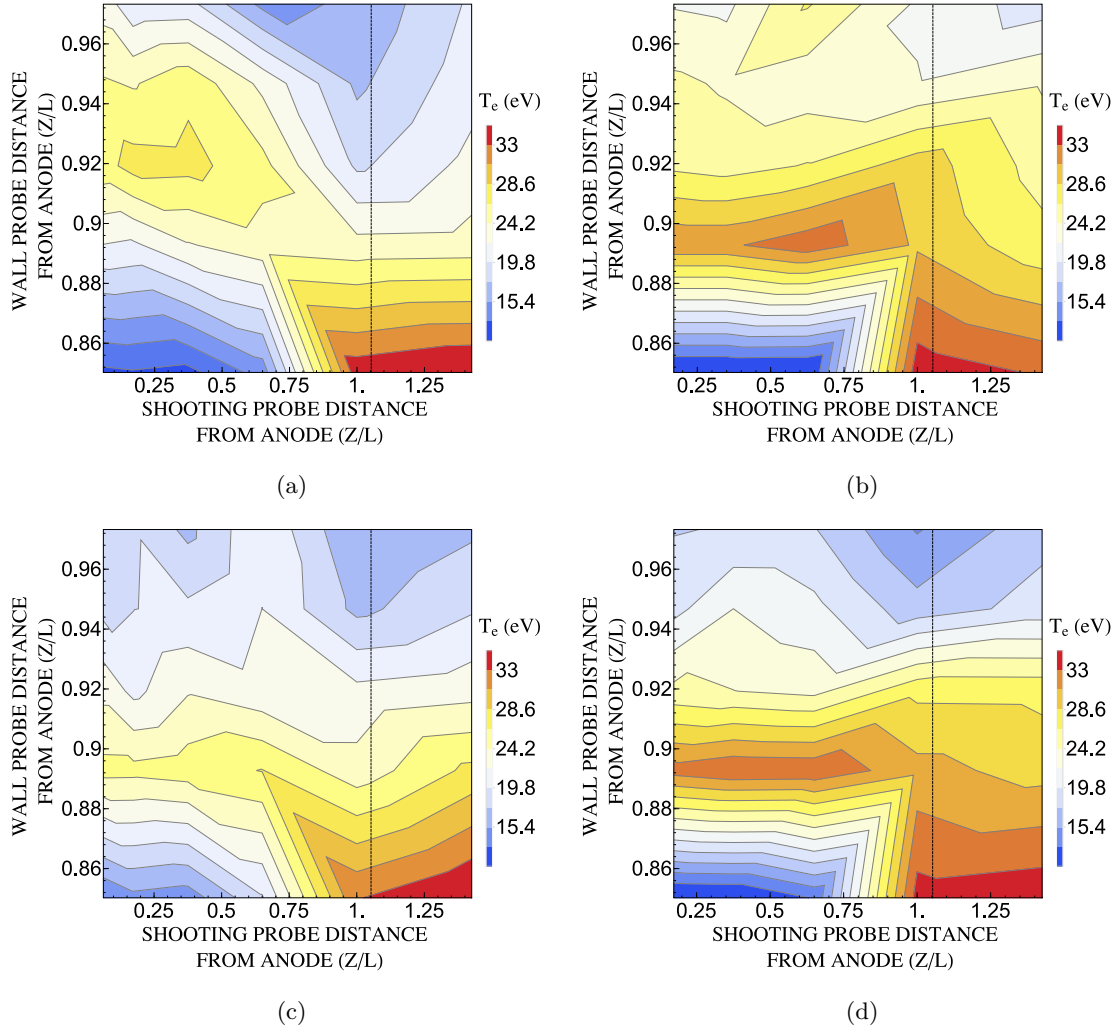


Figure 9: Electron profiles along the inner and outer rings as a function of the scanning probe distance from the anode. (a) Electron temperature at the outer wall as the probe is injected along the outer wall; (b) electron temperature at the inner wall as the probe is injected along the outer wall; (c) electron temperature at the outer wall as the probe is injected along the inner wall (d) electron temperature at the inner wall as the probe is injected along the inner wall. The dotted line in each figure denotes the location of peak radial magnetic field.

To address this possibility, we repeated the same measurements from the previous section with the probe injected along radial locations $X = \pm 0.3 D$, where X denotes the distance from channel centerline and D is the channel width. The results of this study for the electron temperature measurement are shown in Fig. 9, where we immediately can that perturbations still occur even though the scanning probe is off centerline. Significantly, for both cases, the change in the profiles is approximately the same at the inner and outer walls even though the probe is inserted closer to one. This symmetry reflects the fact that the electron equilibration

timescale along magnetic field lines is much faster than the probe transit time. Notably, the shift remains binary in nature with the perturbation occurring at the same point as in the centerline shots ($Z \sim 0.8 L$). However, we can see by comparing Fig. 9 to Fig. 6 that the contortion of the electron temperature profile for the off-axis shots is less pronounced than the centerline measurement. We illustrate this point succinctly by again exploiting the isothermality of lines to map the wall measurements for the unperturbed and perturbed states to the centerline for the three types of shots we performed: centerline, inner wall, and outer wall. The resulting profiles are shown in Fig. 10 where in lieu of plotting the data, we have drawn the interpolated profiles to better illustrate the trends. The plasma is still clearly perturbed by the inner and outer wall shots, which precludes the use of these measurements to infer the correct temperature along centerline. However, the fact that the inner and outer wall shots appear to shift the plasma by a smaller degree lends support to the assertion that the probe perturbations may be driven by plasma density. This is because the plasma is more sparse at the walls. We reserve a full discussion of this for Sec. IV.

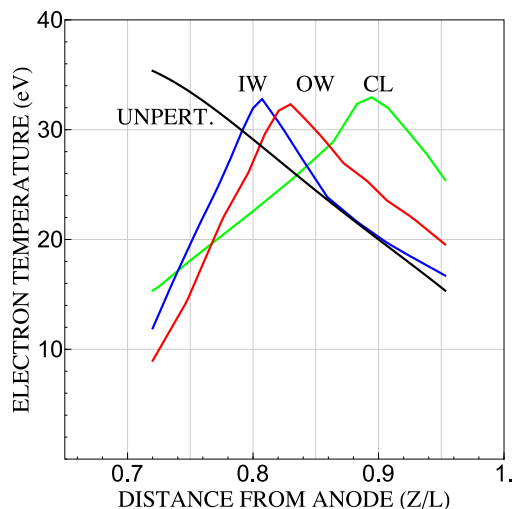


Figure 10: Interpolated electron temperature profiles along centerline as inferred from wall probes. The unperturbed profile is contrasted with the perturbed states that result when the probe is shot along the centerline (CL), inner wall (IW), and outer wall (OW).

2. Effect of probe speed

We next turn to the question of probe speed since increasing this factor may mitigate perturbative effects. This was found to be the case in Ref. 8 where it was shown that employing a high-speed system reduced the perturbations caused by material ablated from the probe insulator. Since the studies we outlined in the previous section were performed at the maximum probe speed available for our system, we instead investigated the effect of lowering the speed. The rationale for this was that if the perturbations increased at lower probe insertion speed, then we could conjecture that improvement may be realized from increasing the speed above the maximum value available to us. We thus contrasted our baseline case for a maximum probe speed on centerline of 90 cm/s with a low speed case of 30 cm/s. We did not go to speeds lower than this out of concern that the probe may become damaged due to a long residence time in the plasma.

We show in Fig. 11 the electron temperature contour plots for the probe speed investigation. Contrasting these results with Figs. 6(a) and (b), we can see that both the degree of the perturbation and the location where it occurs remain unchanged by lowering the probe speed by a factor of three. Fig. 12 clearly illustrates this point by overlaying the average perturbed profile for the maximum probe speed case (90 cm/s) with the lower probe speed (30 cm/s). The two profiles are almost indistinguishable, suggesting that the factor of three change in probe speed did not impact the induced perturbation. This result would seem to suggest that the benefit described in Refs. 8 and 9 from increasing speed to reduce the thermally-induced probe ablation has already been realized at 30 cm/s. Instead, the perturbative effects that led to the shifts we observed in this section and the previous sections must be the consequence of a faster acting process. Enhanced secondary

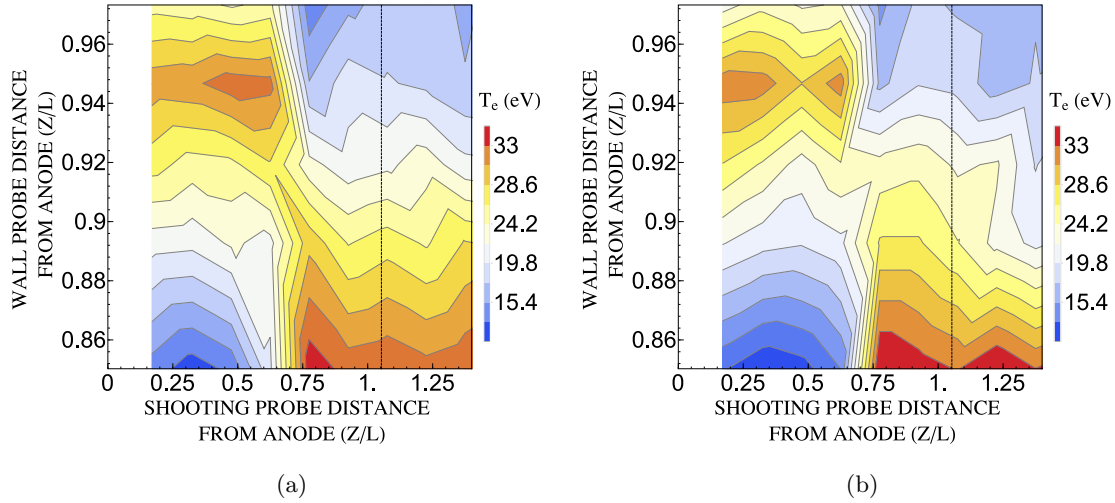


Figure 11: Electron temperature contour plots for a translating probe on centerline moving at 30 cm/s (1/3 the maximum probe speed). (a) Spatial profile at the outer wall. (b) Spatial profile at the inner wall.

electron emission, for example, occurs on the electron thermal time scale which is orders of magnitude higher than the probe transit time. If this is indeed the driving factor, there is no physical probing system fast enough to reduce the types of perturbations in plasma parameters we have observed. Increasing probe speed above the values available to us therefore does not appear to be a viable mitigation technique.

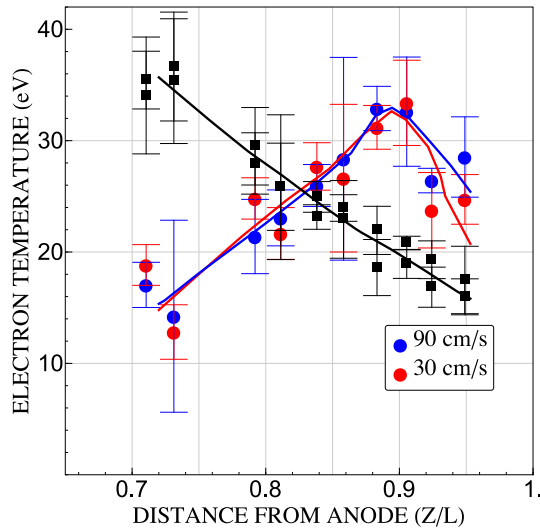


Figure 12: Average spatial dependence of the electron temperature at the centerline as inferred from the inner and outer wall probes. The two cases shown are for maximum speed injection (90 cm/s) and the slow shot case (30 cm/s) and are contrasted with the unperturbed profile

3. Effect of operating conditions

The results outlined in the previous sections suggest that it may not be possible to generate the unperturbed measurements necessary to validate a thruster model for the H6US at the at the nominal condition of 300 V and 20 A. This may not be the case for lower operating powers, however. We conjectured in the radial position study in Sec. III.C.1 that the reduced density at the walls led to a situation where the probe perturbations

were in part, though not entirely, mitigated. Following this reasoning, we can ask the question: are there more benign operating points where probe perturbations are reduced or in fact disappear? If we can identify such an operating point, then it would be possible to use the probe results to inform and validate the models for this condition. With the validated model, we could then extend the results to the desired operating points. This would preclude the need to actively probe the troublesome, high-power condition.

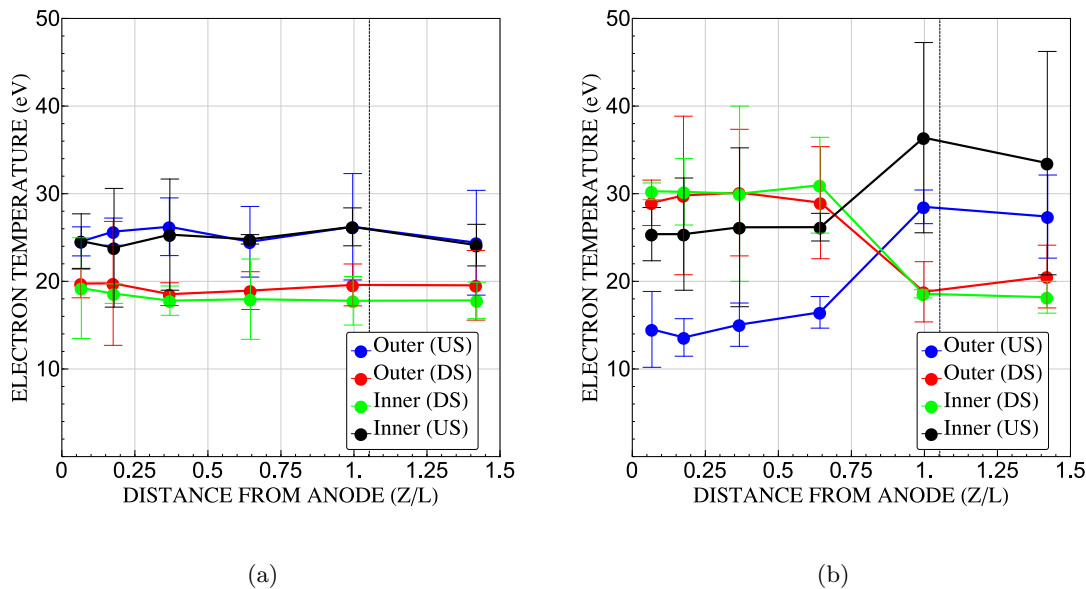


Figure 13: Electron temperature indicated by the two most upstream (US) and downstream (DS) probes on the inner and outer rings as the translating probe entered the channel along centerline. (a) Thruster operating at 200 V and 3 A and (b) thruster operating at 300 V and 10 A

With this purpose in mind, we examined the impact of changing discharge voltage and current on the probe perturbations. In lieu of generating the full electron temperature profile along both walls for each operating point, we instead quantified the impact of the scanning probe insertion on the four wall probes furthest upstream and downstream on each ring. Drawing on our results from the previous sections, we anticipated these locations would exhibit the largest changes in temperature and therefore would serve as valid indicators for the degree of perturbation in the plasma. We show in Fig. 13 two limiting cases—300 V and 10 A and 200 V and 3 A—for the four probes as the translating probe entered the channel along centerline. It is evident that for the lower power case that there was no significant perturbation. This supports the hypothesis that power density and voltage may drive the induced perturbations in the plasma. We can quantify this trend more generally by examining as a function of voltage and current the percentage change in electron temperature induced at each wall probe as the translating probe was injected into the chamber. To this end, we calculated for each of the four probes $|T_{e(p)} - T_{e(0)}|/T_{e(0)}$ where $T_{e(0)}$ is the electron temperature when the probe is downstream of the transition and $T_{e(p)}$ is the temperature upstream of the transition. We then averaged this parameter over all four probes. The resulting trends are shown in Fig. 14(a) as a function of discharge current and at two fixed voltages. It is evident from this plot that reducing the current at fixed voltage mitigates the effect of the probe perturbation. At fixed current, however, reducing the voltage appears to have an even more pronounced effect—moving from 50% to 20% at the discharge current of 10 A. We discuss a possible explanation for this trend in more depth in Sec. IV.

We can relate these results to previous work that has been performed to assess probe induced perturbations in the thruster. For example, Haas et al.^{8,9} and Staack et al.¹⁰ both examined changes in overall discharge current to determine if and when probe perturbations were induced. For our study, we monitored a separate global parameter, the cathode to ground potential, as the probe entered the plasma. We show in Fig. 14(b) the percentage change in this parameter between the perturbed and unperturbed states as a function of the same operating conditions exhibited in Fig. 14(a). While at the higher voltage setting, the perturbations in electron temperature appear to track the changes in the cathode to ground potential, at the lower voltage (200 V), the trends between this global parameter and the temperature profile diverge.

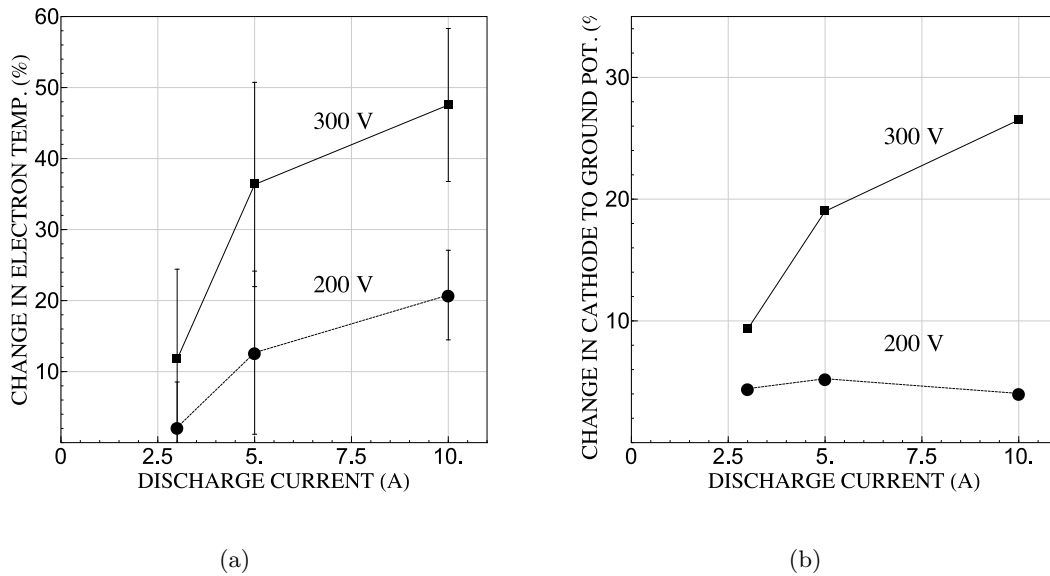


Figure 14: (a) Average percentage change in electron temperature as a function of discharge current induced on the two upstream and downstream probes are the inner and outer rings. (b) Average change in cathode to ground potential resulting from probe injection. In both cases, the probe entered the discharge chamber along channel centerline.

Indeed, an examination of the cathode to ground potential would seem to suggest that the probe insertions are minimally invasive over all the currents investigated at 200 V; however, our study of the plasma parameters indicate that the plasma parameters are still impacted by the scanning probe. Minimizing the changes in global operating thus are a necessary condition for mitigating probe perturbations, but this process is not sufficient to guarantee the plasma parameters are not being changed. This draws into question claims about unperturbed probing that have only relied on the global operating metrics.

In summary, based on our assessment of the changes in the readings on the four wall probes, it does appear to be possible to achieve operating conditions where probe perturbations are minimized. This provides a measure of optimism for identifying conditions where thruster models can be accurately validated.

IV. Discussion

We examined empirically in the previous sections how probe perturbations are impacted by location, speed, and operating condition. We turn now toward determining if there are any overarching guidelines for what useful information can be gleaned from a probe study of the plasma. To this end, we first review our experimental observations in the context of identifying the driving mechanism for the perturbations. We then use the conclusions from this discussion to outline possible mitigation techniques.

A. Discussion of experimental results

Probe speed

As we saw in Sec. III.C.2, probe speed does not appear to be a factor driving the perturbations. This is in keeping with the interpretation that the injection speed is sufficiently high to prevent the insulator ablation Haas et al. noted could occur at low probe speeds.^{8,9} A faster plasma effect—perhaps acting on electron timescales—must be responsible for the observed perturbations. Given the work performed by Staack et al.,¹⁰ the likely candidate for this high-speed process is secondary electron emission (SEE).

Plasma conditions

We found in Sec. III.C.3 that the probe perturbations decrease with current density and discharge voltage. The latter parameter, discharge voltage, has a particularly pronounced effect as exhibited by Fig. 14(a). In the context of the conclusions we drew from the probe speed study, this lends further support to the idea that SEE may drive the perturbations. Indeed, the secondary electron emission coefficient from boron nitride scales as $I_{SEE} \approx n_e T_e^{3/2}$, where n_e is the electron density.²¹ Given the rule of thumb that in the discharge chamber $T_e \approx 0.1V_d$ where V_d is the discharge voltage, the stark dependence of the perturbations on discharge voltage supports the idea that this effect is related to the secondary electrons emitted from the insulating material of the probe. The weaker dependence on discharge current further evidences this point as this current should in principle scale with plasma density, and the SEE current only depends linearly on this parameter.

Location of transition

Previous studies of probe effects have indicated that the maximum perturbation to the global parameters occurs when the probe reaches the electric field peak.^{8,9} This observation is consistent with the idea that secondary electron emission drives the probe perturbations since the electric field is typically coincident with the maximum value of electron temperature. With that said, even though the results from Ref. 8 showed that the maximum perturbation in the discharge current occurred at the electric field peak, this works also indicated (c.f. Fig. 13 in Ref. 8) that the discharge current began to change when the probe was downstream of this location. Our Figs. 9 and 10 indicate a similar trend as the plasma parameters appear to transition when the probe is in range from $Z = 0.8 - 1$ L, and yet the unperturbed electron temperature profile peaks upstream of this transition point at $Z = 0.75$ L. This result has the implication that measurements performed with the injected probe will show the perturbed electron temperature peak and not the true one. By that same token, the estimate for the location of the electric field in Ref. 8 similarly should be shifted. This suggests that while the maximum deviation in discharge current did occur at the measured electric field peak, this peak was in fact the perturbed one. Indeed, the plasma profile was shifted before the probe encountered the electric field maximum.

This conclusion raises an interesting question: if SEE peaks at the electron temperature maximum, how is it possible that the shift occurs before the probe reaches this location? One possible explanation is that it is only necessary for the SEE current added by the probe to exceed a threshold value in order for the perturbation to onset. Once this is achieved, the plasma transitions to the new state. This threshold value may be well below the maximum achieved at the peak electron temperature location, and therefore the lower SEE that occurs downstream of the peak could be responsible for the transition. To illustrate how this could be the case, we note that the effect of SEE is to replace high energy electrons with lower energy ones born from the material interaction with the probe insulator. Since the Coulomb collision frequency scales as $\nu_{ei} \propto n_e (T_e)^{-3/2}$, introducing a lower energy population to the plasma can lower the effective collision frequency. This could in principle change how and where electrons are transported in the discharge chamber—thereby shifting the plasma profile. We motivate how this effect could arise by considering the equation for cross-field electron current density

$$j_{ez} = \frac{q^2 n_e}{m_e \nu_c} \left(\frac{1}{1 + \left(\frac{\omega_e}{\nu_c}\right)^2} \right) E_z, \quad (1)$$

where ω_e is the electron cyclotron frequency, m_e is the electron mass, ν_c is the total collision frequency, and E_z is the electric field in the axial direction. If we assume that the plasma in the discharge chamber is highly magnetized for the electrons, this expression simplifies to

$$j_{ez} = \frac{q^2 n_e \nu_c}{m_e \omega_e^2} E_z. \quad (2)$$

Solving for the electric field, we have

$$E_z = -\frac{v_{ez}}{\nu_c} \left(\frac{qB^2}{m_e} \right), \quad (3)$$

where v_{ez} is the electron drift velocity in the axial direction and B is the magnitude of the magnetic field. This result suggests that the electric field peak, i.e. the region of steepest descent in the plasma potential, is approximately coincident with the location of minimum collision frequency. Similarly, downstream of this peak where the electric field is lower, the collision frequency is higher. Models of the electron collision frequency in the Hall thruster plume (c.f. Ref. 22) confirm this idea as they show the effective collision frequency scales with the electron cyclotron frequency in the plume and then decreases upstream until it achieves a minimum approximately coincident with the electric field peak.

With this in mind, we can use Eq. 3 to find the effect of a collision frequency perturbation (assuming the axial drift remains constant):

$$\frac{\delta E_z}{E_{z(0)}} = \frac{\delta \nu_c}{\nu_{c(0)}}, \quad (4)$$

where $\nu_{c(0)}$ and $E_{z(0)}$ denote the spatial dependence of the collision frequency and electric field before perturbation and $\delta \nu_{c(0)}$ and $\delta E_{z(0)}$ denote the perturbations. Eq. 4 shows how deviations in the initial electric field are directly related to perturbations in the effective collision frequency. If these changes are sufficiently large, e.g. $\delta E_z/E_{z(0)} = \eta$ where η is some threshold value between 0 and 1, a transition may result in the channel plasma. In this case, the criterion for the onset of perturbations would be

$$\frac{\delta \nu_c}{\nu_{c(0)}} > \eta. \quad (5)$$

In the near field, the collision frequency is sufficiently high that even if the probe introduces a relatively high population of SEE electrons, its effect on electron transport will not be realized. As the probe enters the channel, however, the effective collision frequency decreases, and the low temperature electron population from the probe's SEE may be sufficient to satisfy Eq. 5. This may in fact occur before the SEE maximizes $\delta \nu_c$ at the peak electron temperature. Of course, the above argument only serves to illustrate how the shift could occur downstream of the electron temperature/electric field peaks. It does not allow us to predict where the transition occurs or indeed why it results in the apparent downstream shift in the plasma parameters. We would need a full set of plasma measurements (including electron density and drift) as well as a consistent model of the probe SEE in order to estimate this shift. Such a model is beyond the scope of this investigation.

B. Mitigation techniques

The above observations about the probe perturbations—namely the mechanism for the perturbations, its inherent timescale, and the location where it occurs—suggest guidelines for how and when probe measurements are useful for accurately characterizing the plasma. We enumerate in the following these mitigation techniques with their advantages and potential drawbacks.

1. **Determining relevance.** The question of probe perturbations may be irrelevant for many Hall thruster models. Our results showed shifts in the plasma parameters of 15-20% of the discharge channel length, and while this helped resolve important ambiguities concerning the location of the plasma in a magnetically shielded thruster,⁴⁻⁶ measurements for unshielded thrusters may not require the same degree of accuracy. Indeed, accurate modeling is so critical for determining the life of shielded thrusters since they are intended to last for unprecedented timescales. Unshielded thrusters may not have the same lifetime requirements, and since perturbed probe measurements still provide qualitatively correct trends, probe-based measurements may be sufficient to model scaling laws for thrust and to bound estimates on life.
2. **Combining wall and injected probes.** As we showed in Sec. III.B, we can use wall probes in conjunction with translating probes to create an unperturbed spatial profile of electron temperature. This requires combining the scanning probe data on centerline before the perturbation occurs with wall probe data that has been mapped to the centerline. Fig. 8 reveals a potential limitation of this method, however, as we can see that it would be necessary to place additional wall probes in the H6US channel upstream of the rings in order to resolve the location of the electron temperature peak. This likely would be a necessary modification for similarly configured thrusters with temperature peaks near the exit plane. For magnetically shielded thrusters, on the other hand, the combined wall and injected

probe technique may not be viable at all. This is because the peaks in the plasma parameters are shifted downstream of the exit plane and wall probes.⁵

3. **Operating at low power conditions.** As we showed in Sec. III.C.3, lowering the thruster power and discharge voltage can lead to conditions where the perturbations in the plasma are almost negligible. We thus could apply the measurements at these benign conditions toward validating a model of the thruster at the same conditions. The validated model then could be used to extrapolate about behavior at higher power operation. A significant drawback for this technique is that the unknown parameter in thruster simulations that typically drives the need for measurements—the anomalous collision frequency profile—does not necessarily scale predictably with power.²³ Thus, even if the model is benchmarked correctly at a low power, low discharge voltage condition, the validation may not hold for higher power. Moreover, as we showed in the previous section, without a separate metric for measuring the plasma parameters such as wall probes, it is difficult to determine if the plasma is truly in an unperturbed state. Measurements of global parameters such as cathode to ground potential can be misleading.
4. **Reducing probe SEE.** In keeping with the interpretation outlined above for SEE driving the plasma perturbations, reducing the probe SEE coefficient can help mitigate the perturbative effects. This can be accomplished by reducing the probe effective area or changing to lower SEE materials. While there is a lower bound on the size of the probe that can withstand the stress of high-speed injection, Staack and Raitzes had success in insulating their probes in materials with lower SEE coefficients.¹⁰
5. **Optical probing.** A final alternative is to adopt an optical means for probing the plasma such as a Thompson scattering or laser induced fluorescence (LIF). While these diagnostics are inherently more expensive than physical probing and have separate issues in terms of signal to noise problems interpretation, they do offer a method for measuring the plasma non-invasively.

V. Conclusion

We have presented in this investigation a study of how injecting a high speed translating probe into the discharge chamber of a 6-kW Hall thruster perturbs the plasma parameters—potential and electron temperature—that it is designed to measure. At the nominal condition of 300 V and 6 kW, we showed that the perturbation onset when the probe was still downstream of the peaks in electron temperature and plasma potential and that the resulting change could best be described as an abrupt downstream shift in the spatial dependence of the plasma parameters. At the channel centerline, this shift was typically by 10-20% of the length of the discharge chamber. The degree of this perturbation sufficiently explains why different probing techniques in previous studies of this thruster yielded disparate results.^{5,6} It also serves as a proof that for the purpose of validating Hall thruster models, discharge chamber measurements made with injected probes are only accurate to a certain depth upstream of the exit plane. After this point, the plasma can be perturbed significantly.

The knowledge that probing can perturb local plasma parameters raised the relevant question as to when these perturbations occur and if there is ever case when the measurements of the thruster can be trusted. With this in mind, we performed a mitigation study where we showed that while changing probe speed did not appear to have an effect on the perturbations, probing off channel centerline and at reduced power did minimize the magnitude of the perturbations. Taken in the context of previous work that has been performed on probe studies, these latter observations suggested that secondary electron emission from the probe insulator was a major driver for the perturbations. It also emerged from this study that traditional indicators for the degree of perturbation, e.g. monitoring changes in global operating parameters such as cathode to ground potential, are necessary but not sufficient to diagnose whether the probing is changing the plasma. We instead found that in some cases a plasma shift still occurs even when these global parameters do not change. Keeping this metric in mind, we leveraged the results of our mitigation study to arrive at recommendations for how to proceed with probing the plasma in a way that will yield unperturbed measurements. These techniques include employing a combination of wall and injected probes to recreate the unperturbed plasma profile, operating at low power conditions where probe perturbations are minimized, and switching probe configurations to employ lower SEE materials. We of course also recognized that optical techniques, such as spatially-resolved LIF and Thompson scattering, offer the least invasive alternative for probing the plasma.

In summary, high-speed probing has become a staple diagnostic for characterizing the internal properties of Hall thrusters. Yet while high-speed injection does help mitigate some types of probe-induced perturbations, the fact remains that the very act of probing the plasma can change it. The degree of this change may not be significant for benchmarking all types of Hall thrusters, but for the high-power, advanced thruster configurations called for by the next generation of deep space missions, the uncertainty in results yielded by physical probing can represent a major problem. By quantifying this problem, motivating what mechanism drives it, and offering some potential mitigation techniques, however, we have outlined a path for how probe-based measurements can still provide the necessary data for developing these next generation systems.

Acknowledgments

The research described in this paper was carried out at the Jet Propulsion Laboratory, California Institute of Technology, under a contract with the National Aeronautics and Space Administration and funded through the In-Space Propulsion Technologies program. The authors would like to acknowledge Ray Swindlehurst and Nowell Niblitt for their assistance in running the experimental facility.

References

- ¹Strange, N., Landau, D., Polk, J., Brophy, J., and Mueller, J., "Solar Electric Propulsion for a Flexible Path of Human Space Exploration," *Presented at the 61st International Astronautical Congress, IAC-10.A5.2.4, Prague, Czech Republic, Sept-Oct, 2010.*
- ²Brophy, J. and Muirhead, B., "Near-Earth Asteroid Retrieval Mission (ARM) Study," *Presented at the 33rd International Electric Propulsion Conference, Washington, D.C., Oct. 6-10, 2013. IEPC-2013-82.*
- ³Manzella, D. and Hack, K., "High-Power Solar Electric Propulsion for Future NASA Missions," *Presented at the 50th AIAA/ASME/SAE/ASEE Joint Propulsion Conference, Cleveland, Oh. July 28-30, 2014, AIAA-2014-371.*
- ⁴Mikellides, I., Hofer, R., Katz, I., and Goebel, D., "Design of a Laboratory Hall Thruster with Magnetically Shielded Channel Walls, Phase III: Comparison of Theory with Experiment," *48th AIAA/ASME/SAE/ASEE Joint Propulsion Conference & Exhibit, July 30- Aug 1, 2012. Atlanta, GA. AIAA-2012-3789.*
- ⁵Mikellides, I. G., Katz, I., Hofer, R. R., and Goebel, D. M., "Magnetic shielding of a laboratory Hall thruster. I. Theory and validation," *Journal of Applied Physics*, Vol. 115, No. 4, Jan. 2014, pp. 043303.
- ⁶Hofer, R. R., Goebel, D. M., Mikellides, I. G., and Katz, I., "Magnetic shielding of a laboratory Hall thruster. II. Experiments," *Journal of Applied Physics*, Vol. 115, No. 4, 2014, pp. –.
- ⁷Hargus, W. and Cappelli, M., "Interior and Exterior Laser-Induced Fluorescence and Plasma Potential Measurements on a Laboratory Hall Thruster," *Presented at the 35th AIAA/ASME/SEA/ASEE Joint Propulsion Conference, July 20-24, 1999, Los Angeles, CA. AIAA-99-2721.*
- ⁸Haas, J. M., Gallimore, A. D., McFall, K., and Spanjers, G., "Development of a high-speed, reciprocating electrostatic probe system for Hall thruster interrogation," *Review of Scientific Instruments*, Vol. 71, No. 11, 2000.
- ⁹Haas, J. M. and Gallimore, A. D., "Internal plasma potential profiles in a laboratory-model Hall thruster," *Physics of Plasmas*, Vol. 8, No. 2, 2001.
- ¹⁰Staack, D., Raitzes, Y., and Fisch, N. J., "Shielded electrostatic probe for nonperturbing plasma measurements in Hall thrusters," *Review of Scientific Instruments*, Vol. 75, No. 2, 2004.
- ¹¹Haas, J. M., Hofer, R. R., Brown, D. L., Reid, B. M., and Gallimore, A. D., "Design of the H6 Hall Thruster for High Thrust/Power Investigation," *54th JANNAF Propulsion Meeting, Denver, CO, May 14-17, 2007, 2007.*
- ¹²Brown, D., Reid, B., Gallimore, A., Hofer, R., Haas, J., and Larson, C., "Performance Characterization and Design Verification of the H6 Laboratory Model Hall Thruster," *54th JANNAF Propulsion Meeting, Denver, CO, May 14-17, 2007, 2007.*
- ¹³Reid, B., Gallimore, A., Hofer, R., Li, Y., and Haas, J., "Anode Design and Verification for the H6 Hall Thruster," *54th JANNAF Propulsion Meeting, Denver, CO, May 14-17, 2007, 2007.*
- ¹⁴Hofer, R., Goebel, D., and Watkins, R., "Compact LaB6 Hollow Cathode for a 6 kW Laboratory Hall Thruster," *54th JANNAF Propulsion Meeting, Denver, CO, May 14-17, 2007, 2007.*
- ¹⁵Huang, W., Gallimore, A., and Hofer, R., "Neutral Flow Evolution in a 6-kW Hall Thruster," *Journal of Propulsion and Power*, Vol. 27, 2011, pp. 553–563.
- ¹⁶Goebel, D., Jameson, K., and Hofer, R., "Hall Thruster Cathode Flow Impact on Coupling Voltage and Cathode Life," *Journal of Propulsion and Power*, Vol. 28, 2012, pp. 355–363.
- ¹⁷Goebel, D. M. and Watkins, R. M., "Compact lanthanum hexaboride hollow cathode," *Review of Scientific Instruments*, Vol. 81, No. 8, 2010.
- ¹⁸Mikellides, I. G., Katz, I., Hofer, R. R., and Goebel, D. M., "Magnetic shielding of walls from the unmagnetized ion beam in a Hall thruster," *Applied Physics Letters*, Vol. 102, No. 2, 2013.
- ¹⁹Chen, F. F., "Langmuir probe diagnostics," *Mini-Course on Plasma Diagnostics, IEEE-ICOPS Meeting, Jeju, Korea, 2003.*
- ²⁰Hofer, R., Goebel, D., Mikellides, I., and Katz, I., "Design of a Laboratory Hall Thruster with Magnetically Shielded Channel Walls, Phase II: Experiments," *48th AIAA/ASME/SAE/ASEE Joint Propulsion Conference & Exhibit, July 30- Aug 1, 2012. Atlanta, GA. AIAA-2012-3788.*

²¹Goebel, D. and Katz, I., *Fundamentals of Electric Propulsion: Ion and Hall Thrusters*, Vol. 1 of *JPL Space Science and Technology Series*, Wiley and Sons, 2008.

²²Mikellides, I. G. and Katz, I., “Numerical simulations of Hall-effect plasma accelerators on a magnetic-field-aligned mesh,” *Physical Review E*, Vol. 86, No. 4, Oct. 2012, pp. 046703.

²³Jorns, B., Hofer, R., and Mikellides, I., “Power Dependence of the Electron Mobility Profile in a Hall Thruster,” *Presented at the 50th AIAA Joint Propulsion Conference, Cleveland, OH, July 28-30, 2014. AIAA-2014-3620.*